5-2018

Multifunctional Carbon Systems (Interlaminated Carbon Nanofiber Mats/ Carbon Nanotubes Polymer Composites)

Homero Gonzalez Guardiola
The University of Texas Rio Grande Valley

MULTIFUNCTIONAL CARBON SYSTEMS (INTERLAMINATED CARBON NANOFIBER MATS/ CARBON NANOTUBES POLYMER COMPOSITES)

A Thesis

by

HOMERO GONZALEZ GUARDIOLA

Submitted to the Graduate College of
The University of Texas Rio Grande Valley
In partial fulfillment of the requirements for the degree of

MASTER OF SCIENCE ENGINEERING

May 2018

Major Subject: Mechanical Engineering

MULTIFUNCTIONAL CARBON SYSTEMS (INTERLAMINATED CARBON NANOFIBER MATS/ CARBON NANOTUBES POLYMER COMPOSITES)

A Thesis
by
HOMERO GONZALEZ GUARDIOLA

COMMITTEE MEMBERS

Dr. Karen Lozano
Chair of Committee

Dr. Javier Ortega
Committee Member

Dr. Rogelio Benitez
Committee Member

May 2018

ABSTRACT

Gonzalez Guardiola, Homero, Multifunctional Carbon Systems (Interlaminated Carbon Nanofiber Mats/ Carbon Nanotubes Polymer Composites). Master of Science Engineering (MSE), May, 2018, 50 pp, 5 tables, 16 figures, 30 references, 39 titles.

Carbon nanomaterials are an attractive topic within diverse industrial sectors because of their outstanding properties, for example, electromagnetic interference (EMI) shielding effectiveness. Given the broad proliferation of portable electronic and wireless communication devices, the importance of EMI has risen. EMI can be just a nuisance in communications but it can also be catastrophic. The present study develops and analyzes the properties of interlaminated Carbon Nanofiber (CNF) mats/Carbon Nanotubes (CNT) polymer composites towards effective materials to shield EMI. CNF mats were developed using polyvinyl alcohol (PVA) as a precursor, with the Forcespinning® technology to yield nanofibers. The non-woven PVA mats were subjected to a dehydration process followed by heat treatment to develop the CNF mats. The mats were heat pressed with PVA/CNT composite to develop .05 mm thick laminates, which were then staggered and characterized. The highest obtained values were 6 S/cm for electrical conductivity and 50 dB for EMI SE.

DEDICATION

I want to dedicate this work and everything I do in life to my God, who has provided me all the tools needed to succeed and, more importantly, his presence through my journeys. I would also like to share the dedication to my parents, Isabel and Homero, my brother Daniel, and my partner Raquel, who were by my side filling me with patience, comfort and motivation. I owe them all my deepest and greatest gratitude and love.

ACKNOWLEDGEMENTS

I need to give my most sincerer gratitude to my advisor, Dr. Karen Lozano, for promoting an atmosphere of understanding, hard work, learning and creativity. Thank you for giving me the opportunity to work in your lab and introducing me to the incredible world of nanotechnology. And thank you for your advice and friendship, my time invested in the lab and doing research will always be remembered with great pleasure.

I would like to thank Dr. Ortega and Dr. Benitez for their advice and constructive criticism, to future Doctor and my colleague, Claudia Ramirez for her companionship, patience, and guidance, and to my research comrade, Omar Torres for his always words of motivation and mentorship. I also want to thank Dr. Lozano's team of research students and friends, Carlos, Misael, Ydana, Alex and everyone else who assisted and facilitated the use of various instruments in the lab together with their companion. This project is supported by NSF PREM award under grant No. DMR-1523577: UTRGV-UMN Partnership for Fostering Innovation by Bridging Excellence in Research and Student Success.

TABLE OF CONTENTS

Page

LIST OF TABLES

LIST OF FIGURES

Page

CHAPTER I

INTRODUCTION

1.1 Motivation

Electromagnetic interference (EMI) causes degradation/interception and obstruction of the performance of electronic equipment. EMI shielding has been increasing its value over the years given the incredible growth of electronic pollution arising from all the electronic devices being used, especially communication devices. The optimization of EMI shielding effectiveness (SE) is critical in order to adequately protect electronics and confidential data from being damaged. Industry describes that an EMI SE of 40 dB would satisfy 95% of its requirements. This research will focus on utilizing carbon nanofibers (CNF) as the main component to improve electrical and EMI properties.

Carbon materials are already considered a great prospect for EMI shielding because it absorbs and reflects radiation, the two main SE mechanisms. Therefore, the use of carbon nanomaterials would presumably further improve the EMI SE, because of the third and usually neglected SE method, multiple reflections (MR).

One of the issues that might be encountered is that the CNF mats that we pretend to create and use are easily broken because of the small thickness of the mat and the brittleness of carbon. Given such issue, a CNT polymer composite was developed to be embedded into the

CNF mat and enhance its flexibility, maintaining or improving the rest of its properties. The CNT polymer composite used Polypropylene as the matrix with the weight percentage of CNT ranging from 12 to 15. The EMI SE will then be enhanced as well because of the stronger network created by both the CNF and the CNT in the product.

1.2 Main Objectives

The primary purpose of this work proposes the research of the creation of a multilayer system composed of CNF mats and a composite of PP/CNT, which will yield a lightweight and low budget material projected to work efficiently in today's complex industry. The final product is envisioned to excel in conducting electricity and efficiently shielding EMI, though still maintaining their superior mechanical, chemical and thermal properties.

1.3 Detailed Objectives

a Produce carbon nanofibers mats using water-soluble polymer precursors utilizing the Forcespinning® method.

b Carbonize nanofiber mats by exposing them to different temperatures, thus comparing the temperature effect on CNF mat’s properties.

c Prepare polymeric composites by embedding CNF mats into polymer matrices to improve structural properties of the carbonized nanofiber mats as well as to improve handling.

d Create multilayered samples by combining composites films as well as adding carbon nanotubes to the mixtures.

e Measure the EMI SE and electrical conductivity.

1.4 Thesis Structure

The first chapter discusses the background, motivation, and significance of this project. Chapter 2 is a review of the literature focusing primarily on EMI SE. Chapter 3 takes and explains to detail the several techniques utilized in the project. Chapter 4 is a step by step procedure explanation regarding sample preparation and testing methods. The results of the study are exposed and discussed in chapter 5, and chapter 6 is the conclusion of the project, summarizing results. Finally, chapter 7 contains recommendations for continuation on matters of this study.

CHAPTER II

LITERATURE REVIEW

2.1 Electromagnetic Interference

Electromagnetic Interference (EMI) is an electromagnetic signal that, as its name declares, affects other electromagnetic signals by either conduction or radiation. The signals are emitted from devices that transmit, distribute, process, or utilize any form of electrical energy, for example, televisions, computers, cell phones, smart watches, electrical contacts, radios, and radars [1-4]. Now in days, a person traveling by airplane experiences being asked to turn off all electronic devices before takeoff, which is a preventative action towards EMI [5]. EMI will merely continue to be more impactful as time progresses given the incredible speed at which portable electronic devices and wireless communication keep increasing and improving, primarily when the medical and military industries are relying heavily on the sensitivity of such devices [6-7]. The damage caused by EMI toward the equipment can vary from a slight blocking of the equipment's signal to the actual burning of the component's electrical circuit [7]. There are two classifications for the radiation emitted by the EMI, near field and far field.

2.2 EMI Shielding Effectiveness

EMI Shielding Effectiveness (SE) is term given to the attribute of protection and dampening of EMI. Considering not only the present but the increasing impact of EMI concerning all the non-stopping innovative wireless devices coming into the market, proper EMI

shielding has become crucial; however, it continues to be a challenge to be improved [8] [9]. For shielding to be adequate, it is considered that an SE of 40 dB would be enough to satisfy 95% of industry requirements; however, 40 dB shields 99% of incoming EMI [8,10,11]. The shielding must be completely covering the electronic device either emitting or receiving the EM waves because a window will allow propagation, diminishing the SE of the material.

The EMI SE is divided into three principal mechanisms: reflection, absorption and multiple reflections [5,8].

$$SE = R + A + MR \quad (1)$$

Reflection, the primary mechanism of EMI shielding, is the existence of electrons or holes as mobile charge carriers which consistently interact with effect from the electromagnetic radiation [8]. The acquired shield tends to act like it is electrically conducting. However, high conductivity is not required for shielding [5,8,12]. Conduction requires complete connectivity in the conduction circuit while shielding does not. The loss of reflection is a function of the fraction of electrical conductivity (σ_r) by relative magnetic permeability (μ_r), σ_r/μ_r, signifying that the reflection loss decreases with increasing frequency [5,8].

Absorption, the second mechanism of EMI shielding, needs electric and magnetic dipoles which interact with the electromagnetic fields in the radiation [5,8]. The electric dipoles may be provided by materials having high dielectric constants or magnetic permeability, and the loss of absorption can be shown as a function of the multiplication of $\sigma_r\mu_r$, meaning that the loss of absorption increases as the frequency increases [5-8].

The third mechanism is multiple reflections, which is commonly neglected compared with the first two mechanisms [8]. This mechanism benefits from the more significant the surface area is, for example, the more fibers and layers there are in a material, or the more unordered the systems are. The addition of small fillers to a material enhances its shielding effectiveness of EMI by a phenomenon called skin effect, which was found by Chung et al. [8]. Skin effect entails that the near-surface region of a conductive material is the only part that involved with EMI when applied with electromagnetic radiation at high frequencies.

Despite the complete and innovative efforts dedicated to developing polymeric based composites, thin films (a few millimeters) with high shielding effectiveness, the results have shown that SE values higher than 40db are scarce [5,11,13-18]. This thesis concentrated on using a combination of materials and configurations to achieve higher SE while efficiently demonstrating the opportunity of using a cost-effective polymer precursor and manufacturing method coupled with a material that would result in one with promising properties.

CHAPTER III

EXPERIMENTAL TECHNIQUES

3.1 Forcespinning®

Currently, the Cyclone L-1000 models are the only machines capable of creating fibers with a diameter in the micro and nano range via forcespinning® technology. These systems use centrifugal forces rather than commonly use electric fields. The Cyclone, shown in Figure 1, is an entirely automated tool equipped with a vertical spindle driver that houses an insulated heater system and movable spinneret. The material is fed into the spinneret and forced through the orifices as the spinneret rotates. The system is capable of operating in the range of 1,000 to 20,000 RPM. The developed nanofibers are then harvested in solid form on the surrounding collector device. The machine is controlled through an advanced Control Interface, which allows management of various features such as, the spinneret RP, batch run-time, and closed-loop heater output, deposition system, IR and VCS fan parameters.

Figure 1. Cyclone L-1000M. The dimensions of the apparatus are 94 cm in width by 69.9 cm in depth and 100.0 cm in height, weighing 136 Kg.

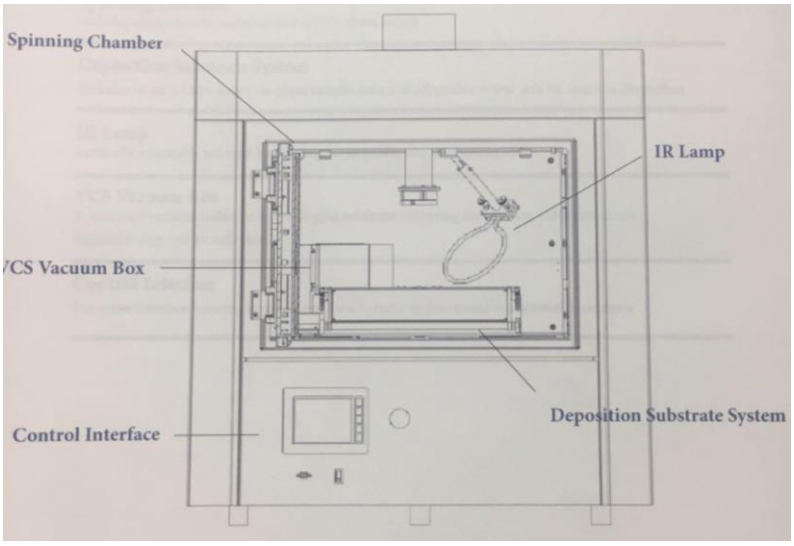

Figure 2. Main system components of Cyclone L-1000.

3.2 Heated Hydrauliced Press

A hydraulic press is a basic machine that exerts force over an area working based on Pascal's principle, where a relatively modest force applied to a cylinder would convert to a more impactful force exerted by a larger cylinder. Figure 3 shows a cross-sectional image of a hydraulic car jack, which employs and can depict the same principle used for a hydraulic press.

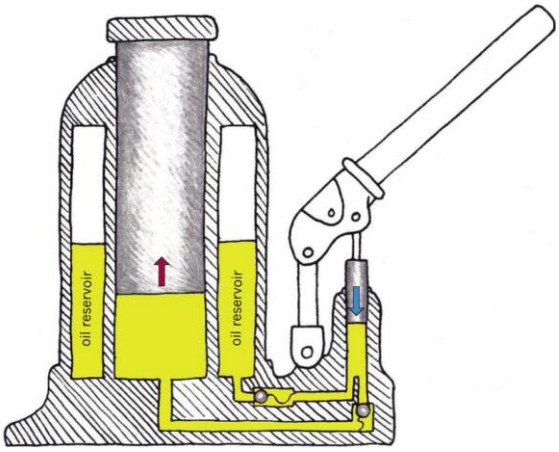

Figure 3. Cross-sectional image of hydraulic system. [19]

The force exerted by the press is used to bend, cut, punch, form and mold materials along with various additional applications. A variant in the hydraulic press may include heated plates, which may aid when dealing with polymeric samples where the content will melt within the applied pressure and set temperature. Thermocouples must be added to control temperature if heated plates are needed on a press to be operated. Hydraulic presses equipped with thermal capabilities also include cooling equipment to control the temperature rate better and be able to cool the part before releasing the applied pressure.

3.3 Stirring Hot Plate

Stirring hot plates are employed in laboratory procedures for precise control of temperature and stirring speed. Figure 4 shows the plate model utilized in the study, the Thermo Scientific Cimarec Stirring Hotplate equipped with a solid aluminum top plate, and it is suitable to be used with glass or metal vessels.

The stirring hot plate is exact and accurate in controlling both thermal and speed properties. The temperature is controlled at the plate surface by an internal sensor, which can heat the plate at temperatures from 30^{o} C to 400^{o} C. The stirring speeds are capable of maintaining from 50 rpm to 1500 rpm.

Figure 4. Cimarec Stirring hot plate.

3.4 Scanning Electron Microscope

A scanning electron microscope or SEM is a microscope that creates an assortment of signals at the surface of samples using a focused beam of electrons [20]. The signals come from how the high energy electrons, normally 40 keV, interact with the atoms of the sample, knocking

out secondary electrons, which then are detected by the microscope to help determine the sample's topography, crystal structure and composition [21]. By using an SEM, it is possible to observe features as small as 0.1 nm [22]. Also, due to how short the wavelength of electrons is, the SEM can capture images with very high magnification and depth, relative to optical microscopes [22].

The SEM is formed by a column, a chamber, and a vacuum system, all connected to software on a computer. The SEM works at vacuum levels. The column has a source or electron gun, two lenses: a condenser and an objective. The chamber holds the sample and the detectors, and often a small camera that provides the user a view of the inside of the chamber. Figure *5* depicts a representation of an SEM and its parts.

The source or electron gun purpose is to provide a stable beam of electron of adjustable energy [23]. The electron gun has a heavy metal filament, usually made out of tungsten, an anode, and a cathode. The electron beam is produced when the tungsten filament is heated, using electrical current, to the point where the electrons create an electron cloud around the filament. Then the electrons are accelerated using a cathode and an anode, where the electrons travel from the cathode to the anode due to the difference in charge. The anode has a hole; when the electron is accelerated towards the anode some electrons pass across this hole, after that, the electrons aligned using an electromagnetic lens [23], forming the beam of electrons. The column has apertures where the beam of electron passes through; the beam is aligned using lenses, a condenser is used to control the diameter of the beam of electron and the objective lenses control the direction and focuses the beam of electrons to the specimen surface. The SEM is held under vacuum conditions to ensure that the electron beam is directed to the specimen and it does not collide with air molecules and atoms. [23] [24]

The specimen is mounted on a holder that can move in all three-dimensional directions; up, down, forward, backward, left, right and tilted to the desired angle. Different phenomena are produced as the electrons from the electron beam collide with the specimen, including backscattered, x-ray emission, secondary electrons, emission of Auger electrons, and absorption of electrons, as shown in Figure 6.

The SEM holds two different detectors, the backscattered and the secondary electrons detector. The backscattered electrons show a flat picture or image of the sample, the production of backscattered electrons is directly proportional to the atomic number of the element present [24]. SEM backscattered images show the topography of the specimen. Secondary electrons are those formed when the electrons from the electron beam collide with the specimen knocking out an electron out of its shell. If these secondary electrons are near the sample surface they will be detected by the secondary detector; therefore, providing high-resolution images that show the morphology of the specimen [24].

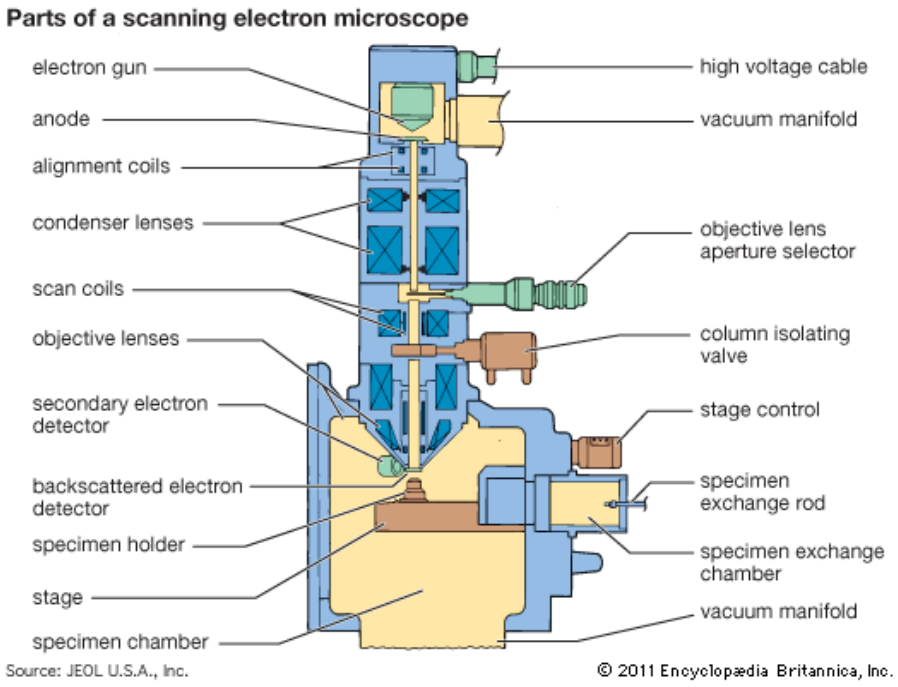

Figure 5. Representation of SEM and its parts.

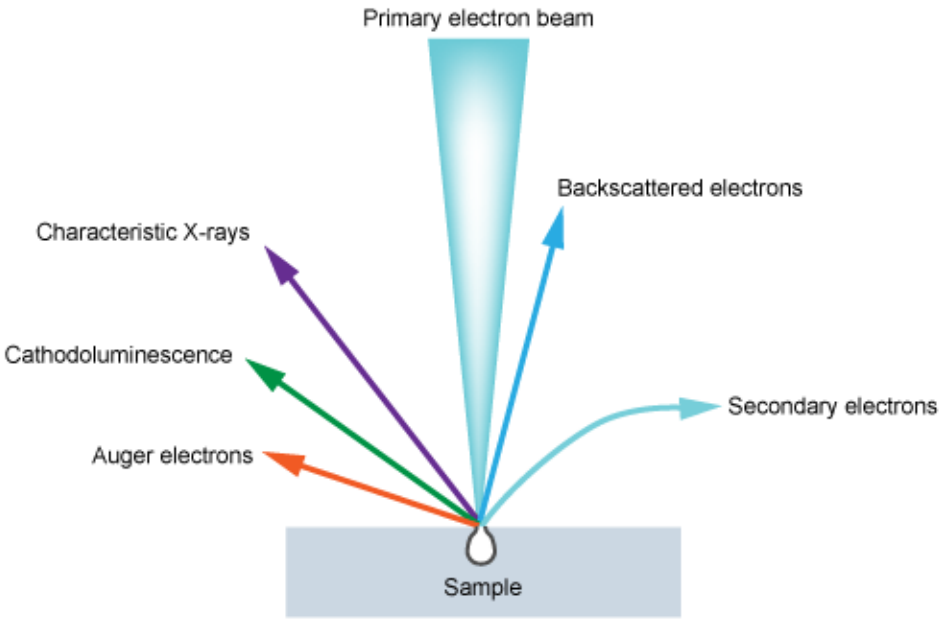

Figure 6. Electron beam interaction diagram. [25]

The SEM electron beam scans the specimen. The sample is scanned from left to right and top to bottom. There is a one-to-one correspondence between the scanning pattern of the specimen and the pattern used to produce the image on the in the computer monitor [23]. All the movements, detector preferences, conditions, and processes are controlled from the computer.

3.5 EMI Shielding Effectiveness

There exist various types of RF network analyzers, which work very differently from one another, but ultimately use the same parameters. The three different RF network analyzers are scalar network analyzer (SNA), vector network analyzer (VNA) and the Large Signal Network Analyzer (LSNA).

The RF network analyzer that was used in this study was the HP 8712 RF Network Analyzer, an SNA. The HP 8712 is optimized for production measurements of reflection and transmission parameters. The instrument integrates an RF synthesized source, transmission/reflection test set, multi-mode receivers, and display. The source features 1 Hz resolution, 50 ms (or faster) sweep time, and up to + 16 dBm output power [26].

Table 1. Measurement Ports Specs. [20]

	HP 8711C and 8712C	HP 8713C and 8714C
Impedance	50 and 75 ohm	
Directivity	40 dB	40 dB
Source match (reflection)	30 dB	30 dB
Source match (response calibration)	14 dB typical	23 dB typical at <1.3 GHz, 20 dB typical at >1.3 GHz
Source match (enhanced calibration)	30 dB	30 dB
Load match	18 dB typical	20 dB typical at <1.3 GHz, 18 dB typical at >1.3 GHz
Reflection tracking	±0.02 dB typical	±0.04 dB typical

Table 2. Source and Receiver Specs [20]

Source

Frequency	
Range	300 kHz to 1.3 GHz (HP 8711C and 8712C) 300 kHz to 3.0 GHz (HP 8713C and 8714C)
Resolution	1 Hz
Stability	±5 ppm 0°C to 55°C (typical)
Accuracy	1) ±5 ppm at 25°C ±5°C 2) <1 Hz at 10% change in line voltage
Harmonics	<–20 dBc, <1 MHz for HP 8711C and 8712C <–30 dBc, >1 MHz for HP 8711C and 8712C <–30 dBc for HP 8713C and 8714C
Output Power	
Resolution	0.01 dB
Level accuracy	±1.0 dB ±1.5 dB Option 1EC[1] ±2.0 dB Option 1E1 ±3.0 dB Option 1EC[1] and 1E1

Maximum and Minimum Power (dBm)

	HP 8711C and 8712C			
	≤1.0 GHz		>1.0 GHz	
Options	minimum power	maximum power	minimum power	maximum power
No options	0	16	0	13
1E1	–60	15	–60	12
1EC[1]	–3	13	–3	10
1DA	–2	14	–2	11
1E1 and 1EC[1]	–60	12	–60	9
1E1 and 1DA	–60	13	–60	10
1EC[1] and 1DB	–5	11	–5	8
1EC[1], 1E1, and 1DB	–60	10	–60	7

Receiver

Frequency range	**HP 8711C and 8712C**
Narrowband	300 kHz to 1.3 GHz
Broadband	0.01 to 1.3 GHz
Dynamic range[2]	
Narrowband	
50 ohm	>100 dB, ≥ 5 MHz (+10 to –90 dBm) >60 dB, <5 MHz (+10 to –50 dBm)
75 ohm	>97 dB, >5 MHz (+10 to –87 dBm) >57 dB, <5 MHz (+10 to –47 dBm)
Broadband	
50 ohm	> 66 dB (+16 to –50 dBm)
75 ohm	> 63 dB (+16 to –47 dBm)
Maximum input	
Narrowband (0.5 dB compression)	+10 dBm
Broadband (0.55 dB compression)	+16 dBm
Damage level	+23 dBm, ±25 VDC
Trace noise[3]	
Medium BW	±0.2 dB
Narrow BW	±0.1 dB

The three-channel, dual mode receivers provide a dynamic range of greater than 100 dB in the narrowband measurement mode. For measurements of frequency-translating devices, the network analyzer features broadband internal and external detector inputs. The receivers incorporate digital signal processing and microprocessor control to speed operation and measurement throughput. Two independent measurement channels and a large CRT display the measured results of one or two receiver channels in several user-selectable formats [26].

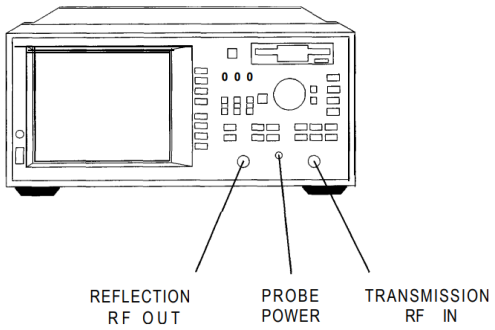

Figure 7. Front panel RF Network Analyzer [19]

3.6 Four-Point Probe Sheet Resistivity

Four-point probes are equipment utilized to measure resistive properties of materials. The instruments are simple to use, having to merely press it against the surface of the material to obtain resultant sheet resistance, R_s, in ohms/square. The way the instruments work is by forcing current through the two outer probes and reading the voltage across the two inner probes as it is shown in figure 8. The probes reside in a straight line and have the same space between them. If the thickness of the material is known, the material resistivity can be obtained by using equation 2, and therefore, the electrical conductivity is obtained from equation 3.

$$\rho = R_s \times t \qquad 2$$

$$\sigma = 1/\rho \qquad 3$$

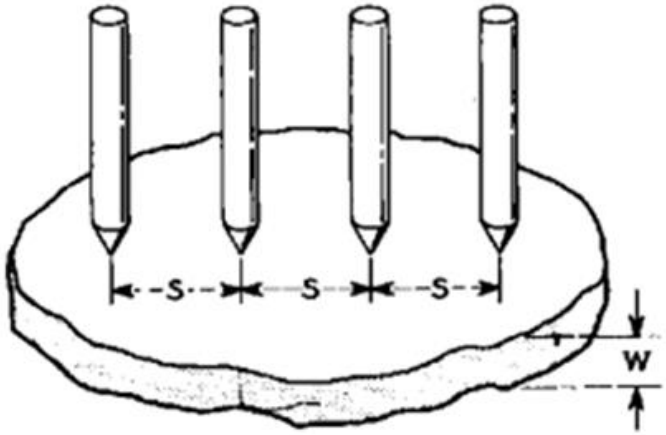

Figure 8. Four-point probe mechanism [28]

CHAPTER IV

EXPERIMENTAL PROCEDURE

4.1 Introduction to Preparations and Procedures

Figure 9 depicts the experimental procedure followed in this project. For the development of nanofibers, polymer solutions were prepared, different concentrations were prepared to analyze its effect of fiber diameter and yield. Nanofibers were then developed by spinning the solution using centrifugal forces. Constant weighing and SEM imagery were employed to determine the experimentation that would follow. The PVA nanofiber mats were then carbonized by exposure to a dehydrating procedure followed by a heat treatment at different temperatures, in order to achieve optimum results. To promote the enhancement of the electrical response, carbon nanotubes (CNT) were used. A solution of CNT was prepared, and the developed carbon nanofiber (CNF) mats were soaked in the CNT solution. To promote ease of handling, the CNF were embedded in resins. Polypropylene pellets were used and pressed against the CNF mats creating layered composites. The samples were characterized at their different stages by EMI SE, SEM, and electrical conductivity.

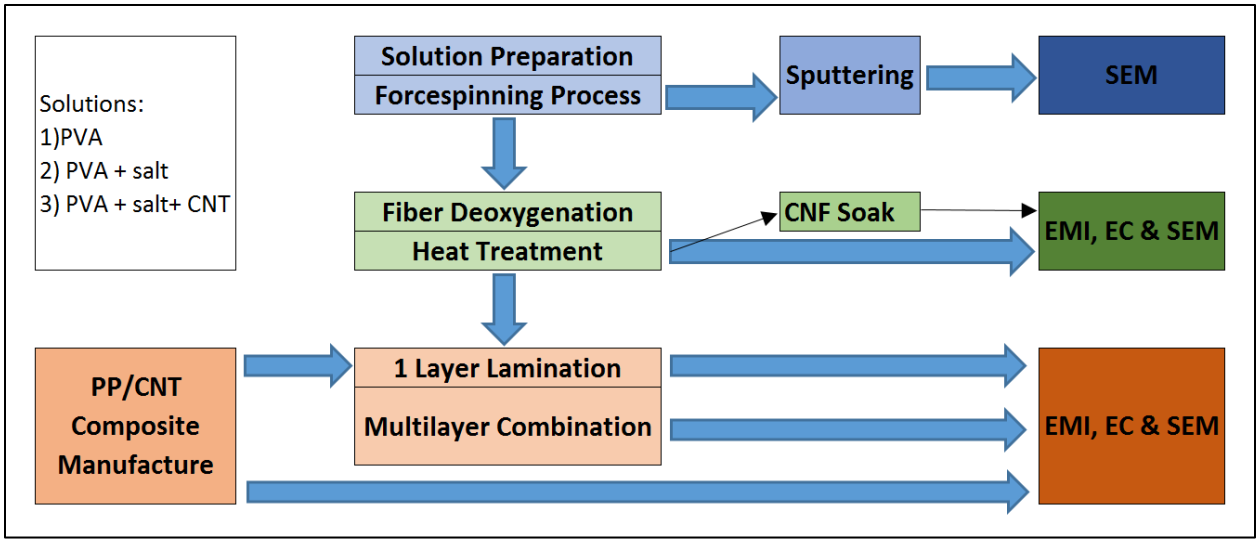

Figure 9. Experimental and Characterization Procedure

4.2 Materials Used

- PVA - Highly hydrolyzed (96%) Polyvinyl Alcohol (Kuraray, POVAL 27-96)
- CNT – Multi-walled Carbon nanotubes with dimensions of 10 nm ± 1 nm × 4.5 nm ± 0.5 nm × 3-~6 μm (O.D x I.D. x L), were purchased from Sigma Aldrich.
- PP - Polypropylene 4280W, having a melting point of 160^{o} C, purchased from Total Petrochemicals
- Sterile Needles – 30-gauge (30G) x ½ in length
- Sulfuric Acid obtained from Fisher Chemical
- Additional materials: Deionized water, Sodium Chloride, Argon, Syringes and Aluminum foil

4.3 Equipment

The equipment employed for this study:

- Thermo Scientific Cimarec Magnetic Stirrer Hot Plate
- Cyclone forcespinning® Machine
- 2 Pyrex Glass 236 mL containers (diameters of 9 cm)
- MTI corporation GSL-1700X Compact Vacuum Tube Furnace
- Thermo Fisher Scientific HAAKE Rheomix Polylab
- Carver Hydraulic Heat Press
- Products Engineering Corporation Digital Caliper

Additional custom equipment:

- Cyclone Spinneret (Figure 10), a customs collector with handle (10 x 10 cm) (Figure 11-a), 1-inch cyclone accumulators (x10) (Figure 11-b), drying net (Figure 12) and an aluminum press molds (Figure 13).

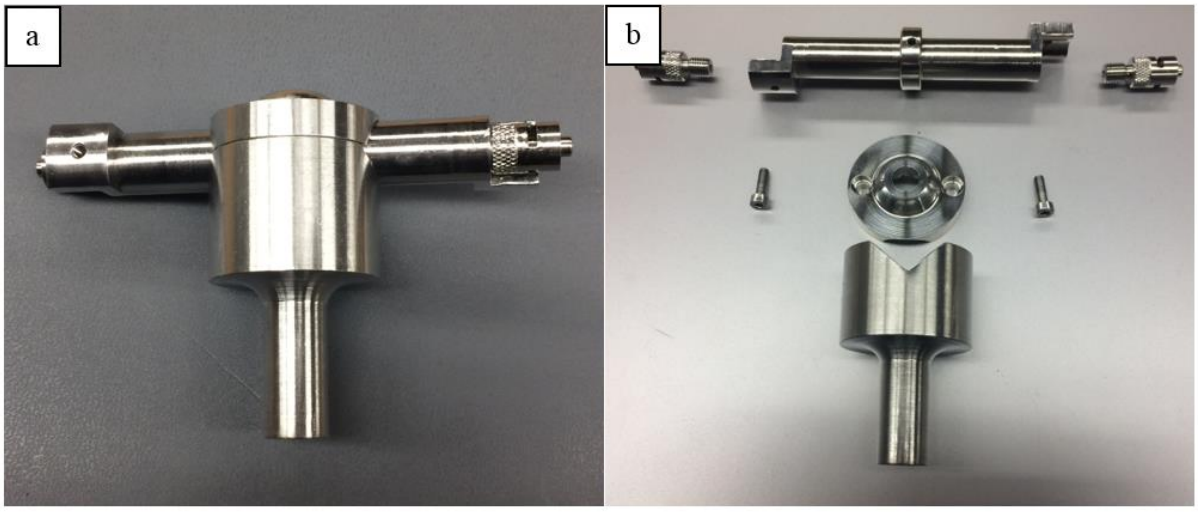

Figure 10. (a) Assembled Cyclone Spinneret; (b) exploded view cyclone spinneret.

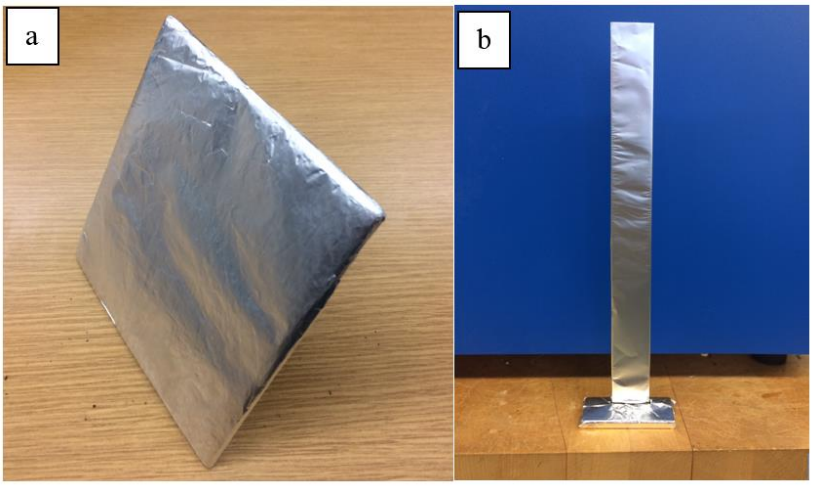

Figure 11. (a) collector where the fibers would be formed into 10x10 mat; (b) accumulator for fibers coming out of spinneret.

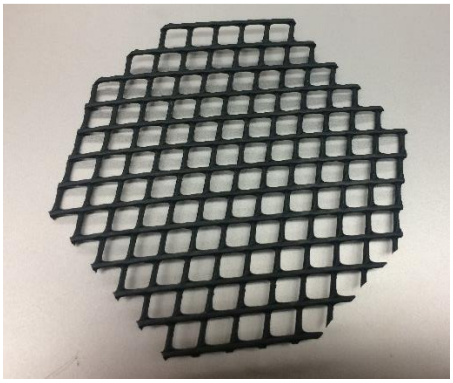

Figure 12. Nets used to hold mats while being washed and while drying

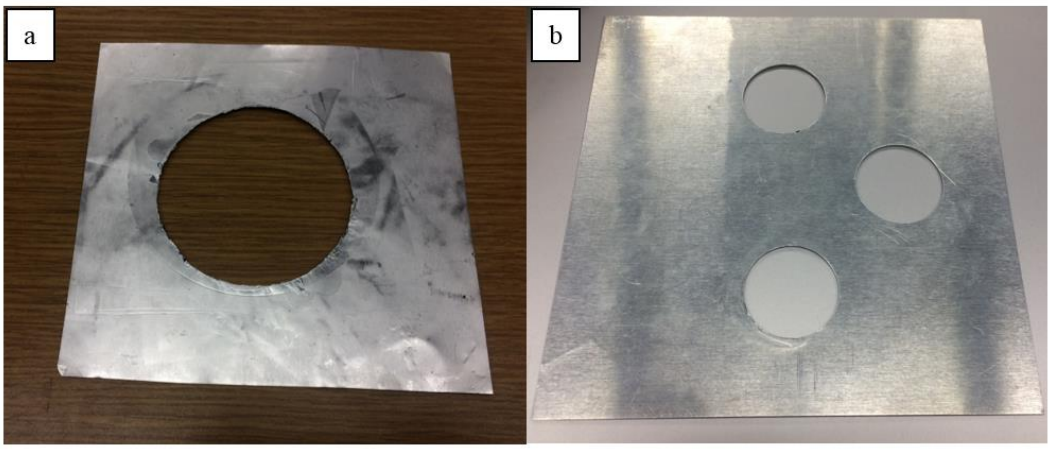

Figure 13. An aluminum mold fabricated to press mats and composites together.

4.4 Precursor Solution Preparation

For optimization purposes, different solutions of PVA and water were prepared to be compared. The base/original solution was prepared using ten weight percent of total weight of PVA in deionized water. The first variant of the solution was changing the PVA weight percentage to 12 weight percent, resulting in a more viscous solution. The next two variations consisted in the addition of sodium chloride to both the first two iterations. The amount of salt implemented was five weight percent to the amount of PVA. The last solutions were prepared by adding CNTs to the four different iterations previously created. The amount of CNT to PVA implemented to the solutions were measured precisely in the following quantities: .05%, .01%, .1%, .25% and 1%. Table does a better job of depicting the different solutions utilized in this research.

Table 3. Description of the solution created

Solutions											
Iteration	Ingredients	Wt. % of Total weight	Wt. % to PVA's wt. %	Iteration	Ingredients	Wt. % of Total weight	Wt. % to PVA's wt. %	Iteration	Ingredients	Wt. % of Total weight	Wt. % to PVA's wt. %
1	PVA	10.000%	-	9	PVA	10.000%	-	17	PVA	10.000%	-
	Water	90.000%	-		CNTs	0.010%	0.10%		CNTs	0.050%	0.50%
					Water	90.000%	-		Water	90.000%	-
2	PVA	12.000%	-	10	PVA	12.000%	-	18	PVA	12.000%	-
	Water	88.000%	-		CNTs	0.012%	0.10%		CNTs	0.060%	0.50%
					Water	88.000%	-		Water	88.000%	-
3	PVA	10.000%	-	11	PVA	10.000%	-	19	PVA	10.000%	-
	Salt	0.500%	5%		Salt	0.500%	5%		Salt	0.500%	5%
	Water	89.500%	-		CNTs	0.010%	0.10%		CNTs	0.050%	0.50%
					Water	89.490%	-		Water	89.450%	-
4	PVA	12.000%	-	12	PVA	12.000%	-	20	PVA	12.000%	-
	Salt	0.600%	5%		Salt	0.500%	5%		Salt	0.500%	5%
	Water	87.400%	-		CNTs	0.012%	0.10%		CNTs	0.060%	0.50%
					Water	87.488%	-		Water	87.440%	-
5	PVA	10.000%	-	13	PVA	10.000%	-	21	PVA	10.000%	-
	CNTs	0.005%	0.0005		CNTs	0.025%	0.25%		CNTs	0.100%	1.00%
	Water	0.9	-		Water	90.000%	-		Water	90.000%	-
6	PVA	12.000%	-	14	PVA	12.000%	-	22	PVA	12.000%	-
	CNTs	0.006%	0.05%		CNTs	0.030%	0.25%		CNTs	0.120%	1.00%
	Water	88.000%	-		Water	88.000%	-		Water	88.000%	-
7	PVA	10.000%	-	15	PVA	10.000%	-	23	PVA	10.000%	-
	Salt	0.500%	5%		Salt	0.500%	5%		Salt	0.500%	5%
	CNTs	0.005%	0.0005		CNTs	0.025%	0.25%		CNTs	0.100%	1.00%
	Water	0.89495	-		Water	89.475%	-		Water	89.400%	-
8	PVA	12.000%	-	16	PVA	12.000%	-	24	PVA	12.000%	-
	Salt	0.500%	5%		Salt	0.500%	5%		Salt	0.500%	5%
	CNTs	0.006%	0.05%		CNTs	0.030%	0.25%		CNTs	0.120%	1.00%
	Water	87.494%	-		Water	87.470%	-		Water	87.380%	-

The following steps were followed for each of the different samples to prepare the precursor solutions:

- PVA and water – PVA and deionized water get carefully weighted to intended weight. PVA is placed in scintillation vial followed by the water, a magnetic pill and the sealing of the vial. The vial is then placed in an oil bath on top of a magnetic stirrer heat plate, where oil is surpassing the level of water inside the vial. The temperature of the oil is set between 65 and 60 degrees Celsius and the RPMs of the magnet to 400. The solution must remain 2.5 hours in the bath and then taken to a stirring plate at room temperature to stay overnight. The solution is then ready for forcespinning®.
- PVA, water, and salt – When incorporating salt into the solution, the salt must be weighted and mixed with the water before PVA is included. For such mixture, the salt, the water, and the magnetic pill are to be placed in the vial and positioned in a stirring plate at 400 rpm at room temperature for 10 minutes. Next, the PVA is to be added to the salt-water mixture and sealed. The vial is then placed in an oil bath on top of a magnetic stirrer heat plate, where oil is surpassing the level of water inside the vial. The temperature of the oil is set between 65 and 60 degrees Celsius and the rpm of the magnet to 400. The solution must remain 2.5 hours in the bath and then taken to a stirring plate at room temperature to stay overnight. The solution is then ready for forcespinning®.
- PVA, water, salt, and CNT – For the addition of CNT, they are to be thoroughly dispersed with the water before the salt is added. To do so, a hand shear mixer is used for 3 minutes. Once the CNTs are well dispersed, salt is added to the mixture with a

magnetic pill and placed on the stirring plate at 400 rpm for five mins. The solution is then remixed with the hand shear mixer for an additional 2 minutes. Next, the PVA is to be added to the dispersed solution and sealed. The vial is then placed in an oil bath on top of a magnetic stirrer heat plate, where oil is surpassing the level of water inside the vial. The temperature of the oil is set between 65 and 60 degrees Celsius and the rpm of the magnet to 400. The solution must remain 2.5 hours in the bath and then taken to a stirring plate at room temperature to stay overnight. The solution is then ready for forcespinning®.

4.5 PVA Nanofiber Development

The creation of the nanofibers consisted in utilizing the forcespinning® method, and therefore the Cyclone machine. First, once the optimal number of accumulators was obtained together with their distance from the center, they are covered by aluminum foil and placed inside of the Cyclone machine. The accumulators were distributed with equal spacing between them. Next, the spinneret gets equipped with a 30-gauge needle on one of its openings. One mL of the solution was injected inside the spinneret using a 5-mL syringe, followed by the placement of the second 30-gauge needle on the remaining opening of the spinneret. It is important to notice that the needles must be changed per run not to allow the concentration of solution inside the needle. The rotational speeds were varied between 5000 to 11000 RPMs depending on the solution concentration and ambient humidity. The time is set for each run allowing the solution to be completely exhausted, varying between 2 – 3 minutes. The collector was passed through the accumulators to collect the fibers that were gathered and stacked after each run. The collector was rotated 90^{o} after each collection to achieve a better distribution of the fibers throughout the mat. The mat had to be 40 g/m^2 to be classified complete.

4.6 Carbonization Process

The carbonation process consists in three steps, an acid treatment followed by a wash and a heat treatment. The acid treatment is meant to infuse sulfuric acid vapors to eliminate oxygenation in the PVA mat, allowing the heat treatments not to damage the mat.

4.6.1 Acid Treatment for Deoxygenation

The acid treatment consists in exposing the PVA mat to sulfuric acid vapors for infusion. To do so, .5 mL of sulfuric acid was distributed inside a glass container. The PVA was then placed on top of the glass container, completely enfolding the opening. An additional glass container was then placed on top of the mat, leaving the mat enclosed between both glass containers. The complete assembly was placed on a heat plate with the temperature set to 180 degrees Celsius. The temperature was then raised in the following manner:

- 15 minutes at 180 degrees Celsius
- 15 minutes at 210 degrees Celsius
- 15 minutes at 240 degrees Celsius
- 15 minutes at 260 degrees Celsius
- 30 minutes at 280 degrees Celsius

Dark spots must me observed in the mat at this point, however, if not, the temperature is to be raised ten additional degrees. The mat must not be moved nor disturbed until the complete area has turned dark. Once the mat was completely obscure, the temperature got lowered to ambient temperature. The specified time/temperature directions were optimized for the fastest time to obtain the desired mat, without damaging it.

4.6.2 Mat Wash

The mat needs to be washed to remove any sulfuric acid inside of the mat. Once the glass containers' temperature was low enough to handle, the mat was removed. Before the washing of the mat, the part of the mat that was not exposed to the vapors was removed, hence leaving the dark, acid treated part of the mat intact. The treated mat was then placed in a stiff net, where deionized water was used to drench the mat. The mat was then turned to be exposed to the water. Finally, the mat was set in a glass container saturated with deionized water in its totality. The bath must last 24 hours, where then it was retrieved to be placed on a net for an additional 24 hours to ensure a completely dry mat.

4.6.3 Heat Treatment

The heat treatment consists of two phases, a pre-heat treatment, and the actual carbonization treatment. The first phase involves placing the mat in a regular oven and setting the temperature to 240 degrees Celsius. Once the desired temperature was achieved and constant for 15 minutes, the temperature was then dropped to ambient temperature. The mat then was placed inside the tube furnace, which was then programmed to rise to a temperature of 850 degrees Celsius for 15 minutes at a rate of 3 degrees per minute. After the 15 minutes, the temperature dropped at the same rate until reaching 500 degrees Celsius. Before the program starts, the tube furnace must be saturated in an inert gas to assure the fibers to be correctly carbonized. 2 hours of a constant flow of argon inside the tube guaranteed that the ambient inside the tube was inert. After the heat treatment, the remaining sample was carbonized nanofibers. The treatment was then repeated with different mats at a temperature of 1000 degrees Celsius.

4.7 CNT Impregnation by Soaking

A small amount of CNF mats created form PVA precursor, were exposed to a CNT soaking treatment to attempt and achieve an impregnation of the CNTs around the CNFs. The impregnation method consisted by first preparing the CNT solution, where 3-parts Tetrahydrofuran (THF) was mixed with 1-part deionized water to later implement .01% CNTs. In order to achieve the best dispersion possible of the CNT in the solution, the hand shear mixer was used for 5 minutes. The solution would then be placed in a larger container where the CNF mat would follow, being exposed to the solution for 1 minute. The CNF mat would then be taken out from the solution carefully and placed in the net to dry.

4.8 PP/CNT Composite

The composite material was created using 12 and 15 weight percent of CNT to PP. The material was blended in the HAAKE Rheomix Polylab System with the Banbury rotors. Before inserting the materials, the HAAKE system had to be programmed to the different temperatures needed with their rpm of the rotors, and the time the material would be getting mixed. The initial temperature and velocity were 150^{o} C and 40 rpm respectively. The material was then inserted in slowly, not allowing it to conglomerate in the necked entrance of the mixer. Once the entire material was inside the mixer, the program would begin. The program consisted in blending the materials at first properties for 10 minutes, followed by an increase in temperature and angular velocity to 165^{o} and 50 rpm. Such conditions were held for 10 additional minutes after which the temperature was decreased to 120^{o} C and the rotors stopped to correctly remove the material from inside the mixer. The final product was a consistent composite of PP/CNT.

4.9 CNF Embedment

Using the heat press and the aluminum molds, PP/CNT composite films were created by applying a pressure of 4.5 metric tons to them and a temperature of 175 degrees Celsius. The film, right side of Figure, was then embedded within a CNF mat of the same size, left side Figure, inside an aluminum mold. The pressing was held for a brief 10 seconds, after which it was released and the mold was removed from the press. The yielded product was consistent with the dimensions of the CNF mat that was used.

Figure 14. (a)CNF mat, left. CNT/PP composite, right

4.9.1 Fabrication of multi-layered carbon Nano-systems

The multi-layered systems consist of a stack of 2, 4 or 8 pre-embedded samples. The embedded CNF samples were stacked inside the mold and put in the press at a temperature of 175^{o} C for 10 seconds before the pressure was provided. The stack was then pressed for 10 seconds to 3 metric tons for a pile of 2, 2.5 metric tons for a stack of 4, or 2 metric tons for a stack of 8. The pressure was then released and mold removed from the press.

4.10 Characterization

The characterization performed in the samples consisted of morphology, electrical conductivity, and electromagnetic interference shielding effectiveness. The instrument employed in this study to observe the morphology of the samples was the Carl Zeiss Sigma VP Scanning Electron Microscope (SEM). The electrical conductivity of the samples was calculated by obtaining the resistivity of the samples using the R-CHEK RC-2175 4-Point Sheet Resistance Meter From EDTM. The shielding effectiveness (SE) of the EMI of the material was measured with a Hewlett Packard RF Network Analyzer 8712C.

In the case HPRF Network Analyzer 8712C used to obtain the EMI SE, the process involves in placing the material in between two fittings connected to the machine by coaxial cables where the electromagnetic emission passes through. The fitting testers, Figure, were developed to improve several aspects of past testing regarding ASTM D4935-99, where the new testers have the capability of going to a higher frequency and utilizing smaller samples [3].

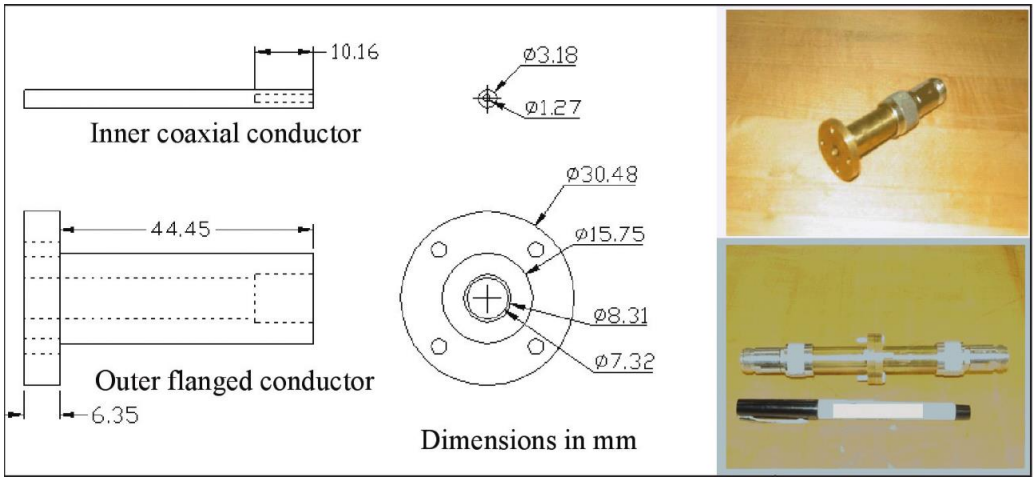

Figure 15. Manufacturing drawings and photos of SE tester developed in UTPA [3].

CHAPTER V

RESULTS AND DISCUSSIONS

The findings obtained in the investigation completed upon the CNF mats, the PP/CNT composites and their combinations will be exposed, analyzed and compared in this section. The first material to be shown will be the SEM characterization of the samples, including the PVA nanofiber mats before becoming CNFs. Afterward, the electrical characterization of the final states of the samples will be presented. The measurements obtained from the EMI SE of the samples will be the last material to be exposed and analyzed.

5.1 SEM Characterization

The imaging obtained for the different type of samples by SEM were sometimes derived from the same sample before or after a specific process was run through it. Figure 16 (a) shows a nonwoven PVA nanofiber, the base sample of the study, and right next to it (b) is the same PVA nanofiber but with the addition of sodium chloride. The only seen difference sodium chloride appears to contribute, are the crystals that are attached to the fibers. However, once the PVA mat with sulfur chloride goes through the heat transfer process, Figure 17, the development of veils between the fibers is achieved.

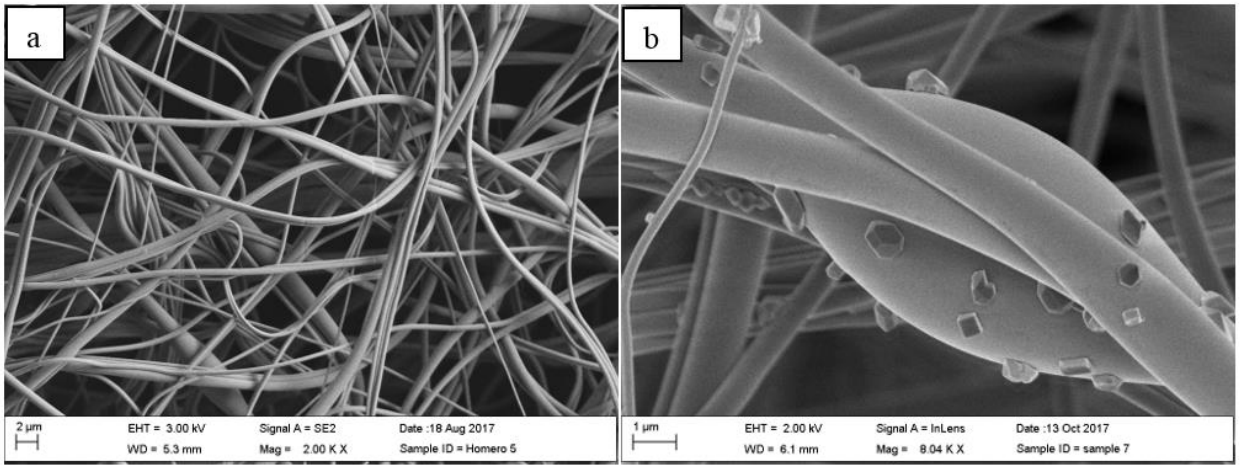

Figure 16. SEM imaging of (a) nonwoven PVA nanofibers; (b) nonwoven PVA nanofibers with salt

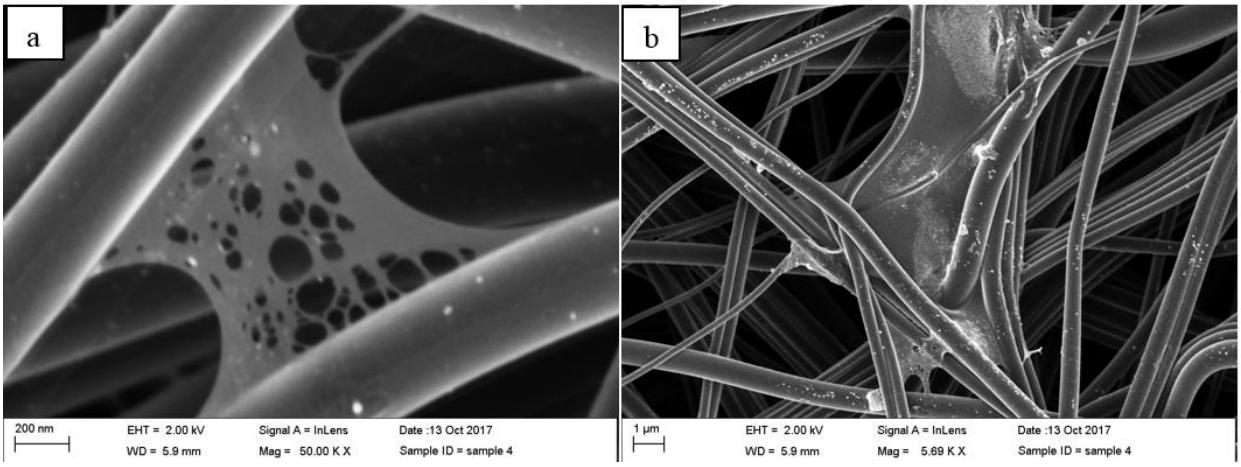

Figure 17. SEM imaging of (a, b) nonwoven mats of the graphene-CNF mat

The impregnation by soaking of CNT into the CNF mats came out to yield a good dispersion of multiwalled-CNT around the CNFs as it is shown in Figure 18. The CNTs are depicted swirling around the CNFs creating more paths to conduct electrons.

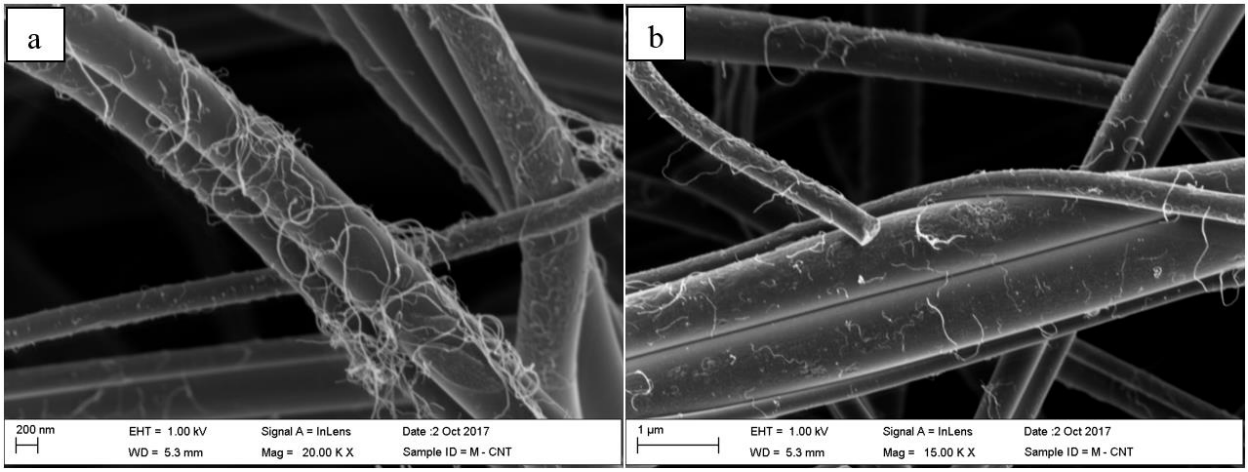

Figure 18. SEM imaging of nonwoven CNF mats impregnated with CNTs

A combination of employing both the graphene-fiber structure together with the impregnation of CNTs was studied. Figure 19 exhibits the graphene-CNF mat impregnated with CNTs, where it can be observed that the number of CNTs was reduced compared to the mat showed in Figure 18.

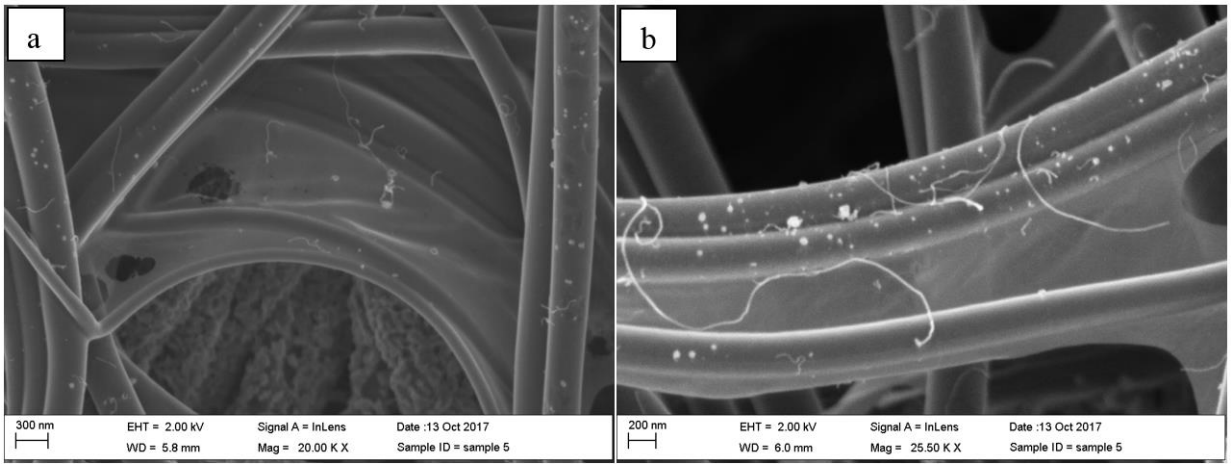

Figure 19. SEM imaging of nonwoven graphene-CNF mats impregnated with CNTs

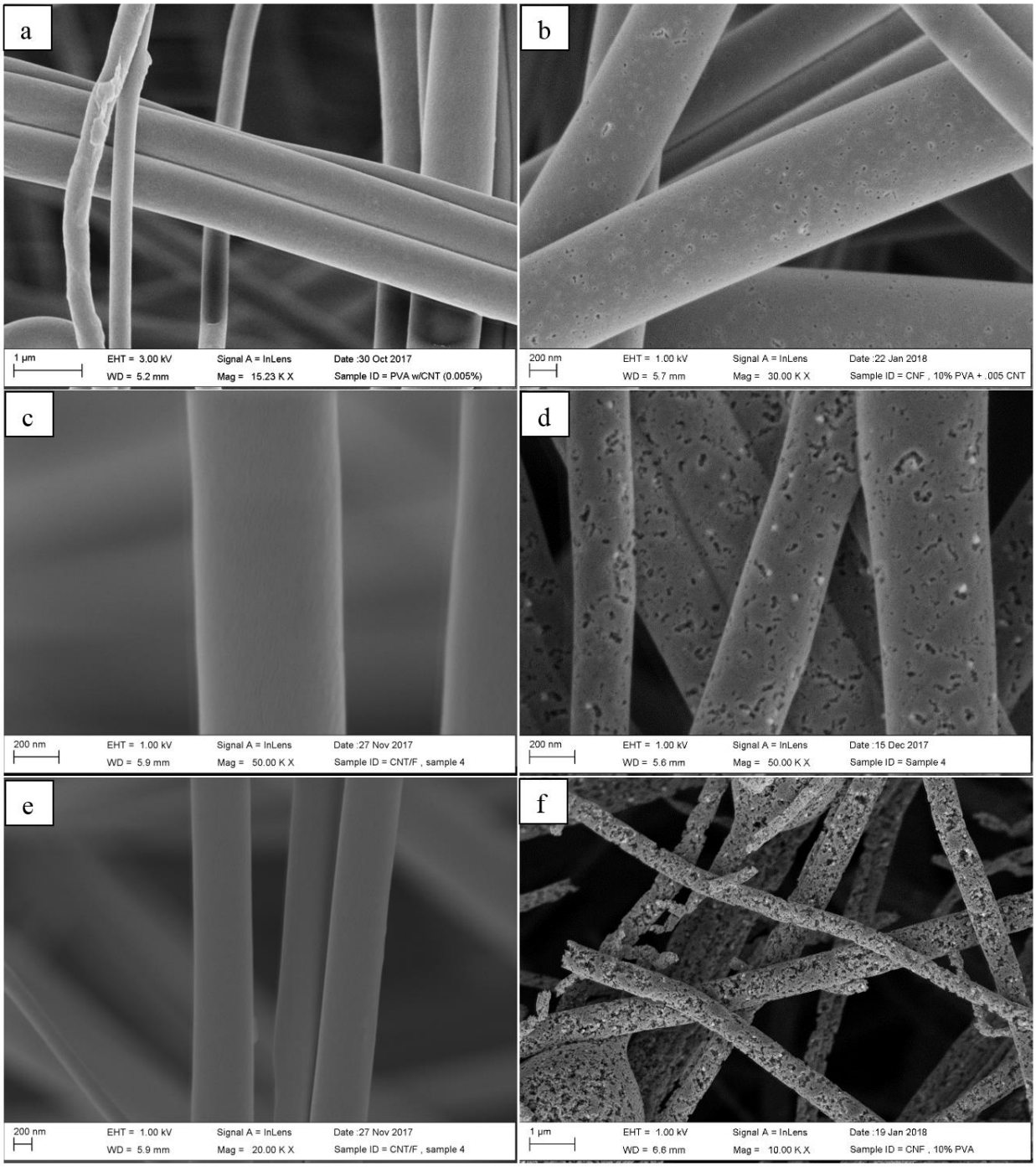

Figure 20. SEM imaging of (a) PVA mat containing .005w.% CNTs; (b) CNF PVA mat containing .005w.% CNTs; (c) PVA mat containing .05w.% CNTs; (d) CNF PVA mat containing .05w.% CNTs; (e) PVA mat containing .1w.% CNTs; (f) CNF PVA mat containing .1w.% CNTs;

The introduction of CNTs to the precursor played the most impact to the surface of the nanofibers, creating voids in the nanofibers. Figure 20 perfectly depicts how the voids in the CNFs surfaces incremented as the number of CNTs used increased.

Figure 21 and Figure 22 depict the CNFs and CNTs surrounded in PP respectively. Emdeding the CNF mats in a polymer, in this case the PP/CNT composite, assisted in making the samples easier to test for EMI SE, given that the CNF mat by itself sheds fibers and it is brittle and with the combination of the composite it becomes more flexible.

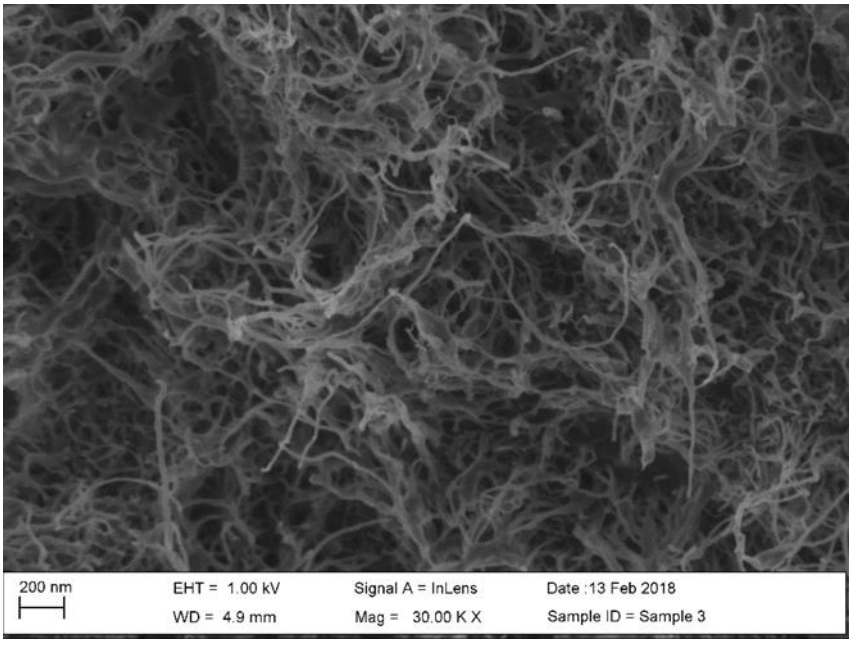

Figure 21. PP/15% CNT composite.

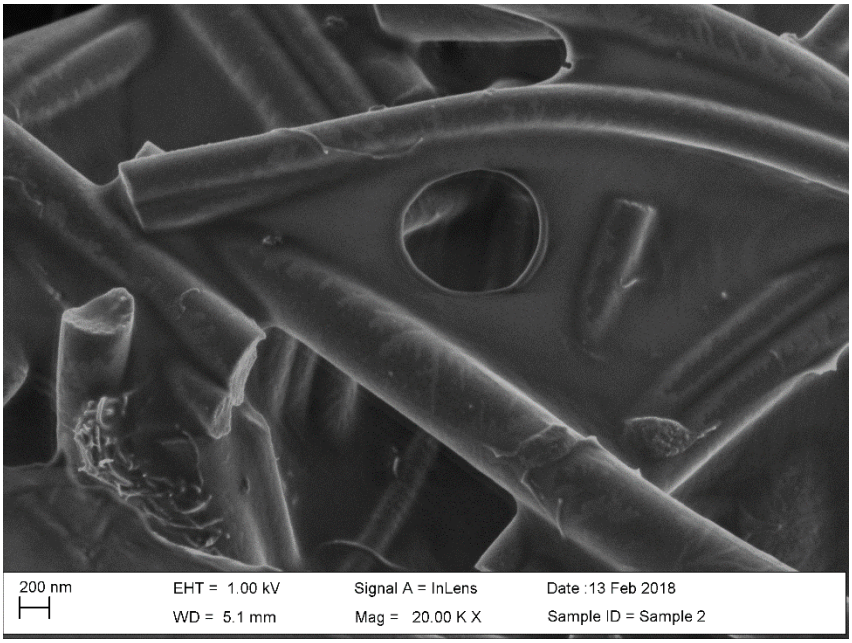

Figure 22. CNFs embedded in PP/CNT composite.

Figure 23 depicts the cross-sectional area of an 8-layered interlaminate carbon system. The sample includes 8 CNF mats brought together by the PP/15% CNT composite. The CNF mats can be distinguished by observing the lighter areas running almost parallel to one another.

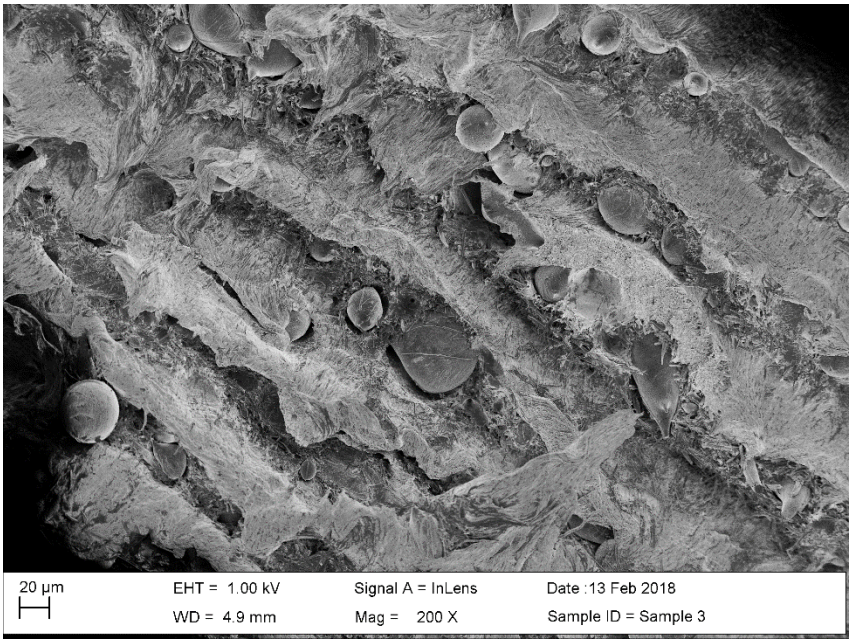

Figure 23. 8-layer interlaminate carbon system

5.2 Electrical Properties

The electrical conductivity values of every sample are exposed in Table 4. The electrical conductivity and resistivity were calculated by measuring the sheet resistance of each sample, using equations 1 and 2.

There are three different categories that the samples could be break into: CNF mats, PP/CNT composite, and the combination of both by interlamination. The base sample mat that sets the investigation is shown as sample 1 in Table 4, a CNF mat fabricate with 10% PVA at a temperature of 850° C, with no salt added nor CNT in solution or impregnation. Such base sample mat contained an electrical conductivity of .28 S/cm.

Table 4. Electrical Conductivity and Resistivity values for samples

#	Description	PVA w/% solution	CNT w/% to PVA	Salt w/%	HT Temp °C	CNT Impreg. after HT	Inter Lam. Layers	Elec. Res. ρ (Ω·cm)	Elec. Con. σ (S/cm)
1	CNF mat	10	0	0	850	0	0	3.604	0.277
2	CNF mat	12	0	0	850	0	0	2.246	0.445
3	CNF mat	10	0	5	850	0	0	2.071	0.483
4	CNF mat	12	0	5	850	0	0	2.029	0.493
5	CNF mat	12	0	0	850	.01% CNTs	0	2.142	0.467
6	CNF mat	12	0	5	850	.01% CNTs	0	1.902	0.526
7	CNF mat	10	0	0	1000	0	0	0.913	1.096
8	CNF mat	12	0	0	1000	0	0	0.510	1.960
9	CNF mat	10	0	5	1000	0	0	0.759	1.317
10	CNF mat	12	0	5	1000	0	0	0.424	2.359
11	CNF mat	10	0.005	0	1000	0	0	0.424	2.358
12	CNF mat	10	0.005	5	1000	0	0	0.427	2.342
13	CNF mat	10	0.01	0	1000	0	0	0.416	2.404
14	CNF mat	10	0.01	5	1000	0	0	0.415	2.410
15	CNF mat	10	0.025	0	1000	0	0	0.411	2.431
16	CNF mat	10	0.05	0	1000	0	0	0.376	2.658
17	CNF mat	10	0.1	0	1000	0	0	0.356	2.813
18	Comp.PP/12%CNT	0	0	0	0	0	0	1.428	0.700
19	Interl. PP/12%CNT	12	0	5	850	0	1	2.709	0.369
20	Interl. PP/12%CNT	12	0	5	850	0	2	1.028	0.972
21	Interl. PP/12%CNT	12	0	5	850	0	4	0.992	1.008
22	Interl. PP/12%CNT	12	0	5	850	0	6	0.917	1.091
23	Interl. PP/12%CNT	12	0	5	850	.01% CNTs	4	1.080	0.926
24	Comp.PP/15%CNT	0	0	0	0	0	0	0.670	1.492
25	Interl. PP/15%CNT	12	0	5	850	0	1	0.519	1.928
26	Interl. PP/15%CNT	12	0	5	850	.01% CNTs	1	0.550	1.819
27	Interl. PP/15%CNT	10	0	0	0	0	1	0.354	2.825
28	Interl. PP/15%CNT	10	0.005	0	1000	0	1	0.306	3.270
29	Interl. PP/15%CNT	10	0.01	0	1000	0	1	0.284	3.524
30	Interl. PP/15%CNT	10	0.025	0	1000	0	1	0.288	3.472
31	Interl. PP/15%CNT	10	0.05	0	1000	0	1	0.262	3.818
32	Interl. PP/15%CNT	10	0.1	0	1000	0	1	0.226	4.433
33	Interl. PP/15%CNT	10	0.05	0	1000	0	2	0.225	4.444
34	Interl. PP/15%CNT	10	0.1	0	1000	0	2	0.204	4.902
35	Interl. PP/15%CNT	10	0.05	0	1000	0	4	0.210	4.762
36	Interl. PP/15%CNT	10	0.1	0	1000	0	4	0.188	5.322
37	Interl. PP/15%CNT	10	0.05	0	1000	0	8	0.173	5.787
38	Interl. PP/15%CNT	11	0.1	0	1000	0	8	0.165	6.061

5.2.1 CNF mats

The first category is composed of samples 1-17, and they are CNF mats with variations of PVA percentage used in solution if either .5% salt was used on the solution or not, CNT percentage used in solution, CNT soaking impregnation of CNF mat and temperature of the heat treatment. All the samples in this category contained a thickness of .08-.09 mm. Every electrical conductivity value obtained with the addition of salt, CNTs, additional PVA or the increase of temperature increased from that of the base CNF mat, sample 1.

The increment of the percentage of PVA to water from 10% to 12 % in the initial solution encourages a higher electrical conductivity of the mat, which can be observed when comparing base sample mat 1 and sample mat 2 in Table 4. The conductivity of the CNF mat is increased from 2.77×10^{-1} to 4.45×10^{-1} S/cm. The higher conductivity arises because the velocity used to create the samples is improved with a more viscous solution, therefore yielding fibers with a smaller diameter. Because the weight of all the mats was congruent with each other, thinner fibers mean a higher density in the fiber network.

Like previously mentioned in the SEM imaging section, the addition of salt in the PVA solution promotes the creation of graphene veils between the fibers [29], which act as “bridges” or a cross-link for the fibers. Given the values obtained for the samples, the graphene veils contribute to the increase in electrical conductivity which is demonstrated when comparing the base mat, sample 1, with sample mat 3, where the conductivity almost doubles to a value of 4.83×10^{-1} S/cm.

The addition of CNTs to the CNF mats was tested using two different approaches, the first being the impregnation by soaking of the CNF mat in a CNT solution to disperse the CNT around the CNFs and the second approach consisting in implementing the CNTs inside the PVA solution before the CNF mats are created. For the first approach, the maximum CNTs amount that could be used for the impregnation before no extra value was added was .01% of CNTs. An increase of electrical conductivity was achieved by this method, and it can be observed when comparing sample mat four against sample mat 2. Both mats were created utilizing 12% PVA as the precursor, and were treated at the same temperature of 850° C; therefore the only difference was the impregnation of CNT. The conductivity increased from 4.45×10^{-1} to 4.67×10^{-1} S/cm.

The most significant electrical conductivity value obtained in category 1 was of 2.81 S/cm, and it pertains to sample mat 17 from Table 4, the CNF mat with 10% PVA used in the solution together with a .1% of CNT per PVA and heat treated to a temperature of 1000° C. Comparing sample mat 17 with the base sample mat 1, the conductivity was raised for one order of magnitude, from 2.77×10^{-1} to 2.81×10^{0} S/cm. This approves that the inclusion of CNT in the solution dramatically improves the electrical conductivity of the mat much more than the integration of CNTs by the soaking impregnation method. Figure 24 depicts the trend followed by the sample mats 1, 11, 13, 15, 16 and 17, which contain 0, .005, .01, .025., .05 and .1 percent weight of CNT to PVA respectively. The difference is notable from the base sample mat 1, which lacks CNT, to sample mat 11; however, the difference between the rest of the samples is negligible after the first jump. This shows that the CNT inclusion to the precursor serves as additional pathways for the conduction of the electrons.

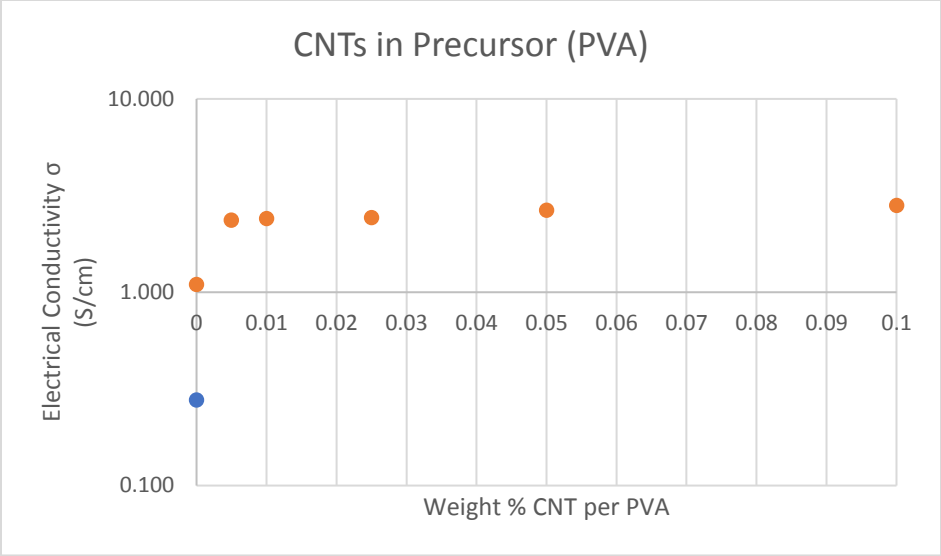

Figure 24. Percentage of CNTs added to precursor vs. electrical conductivity. Blue data point indicates sample prepared at 850°C and orange data points indicate samples prepared at 1000° C.

5.2.2 PP/CNT Composite

The electrical conductivity of the two composites employed in this study, 12 and 15 percent weight CNT, can be observed in Table 4, sample mats 20 and 26 respectively. The increment of 3 weight percent doubles the conductivity, creating a better composite to aid in the bridging of electrons.

5.2.3 Interlaminate Carbon Systems

The third category consists of the combination of all iterations of both the CNF mats and the PP/CNT composites. The category is depicted by the green area in Table 4, where it can be observed how each layer impacts the conduction of electricity. Figure 25 portrays how each layer of CNF mat and PP/CNT composite influences the conductivity of the samples. Figure 25 employs sample mats 17, 32, 34, 36 and 38, which are the samples created by CNF mats containing .1 weight percent CNTs to PVA in the precursor and carbonized at 1000° C, and

PP/15% CNT composite. When creating one layer interlaminate system, the embedment of composite inside the mat would have the thickness remaining the same as the one measured of the CNF mat, meaning the polymer completely immerses inside of the mat. Once the additional layers of CNF mats are added to the equation, the thickness starts to increase, but it would not double completely. The thicknesses of the interlaminate systems were averaged as follow:

- 2-layer interlaminate carbon system: .16 mm
- 4-layer interlaminate carbon system: .30 mm
- 8-layer interlaminate carbon system: .65 mm

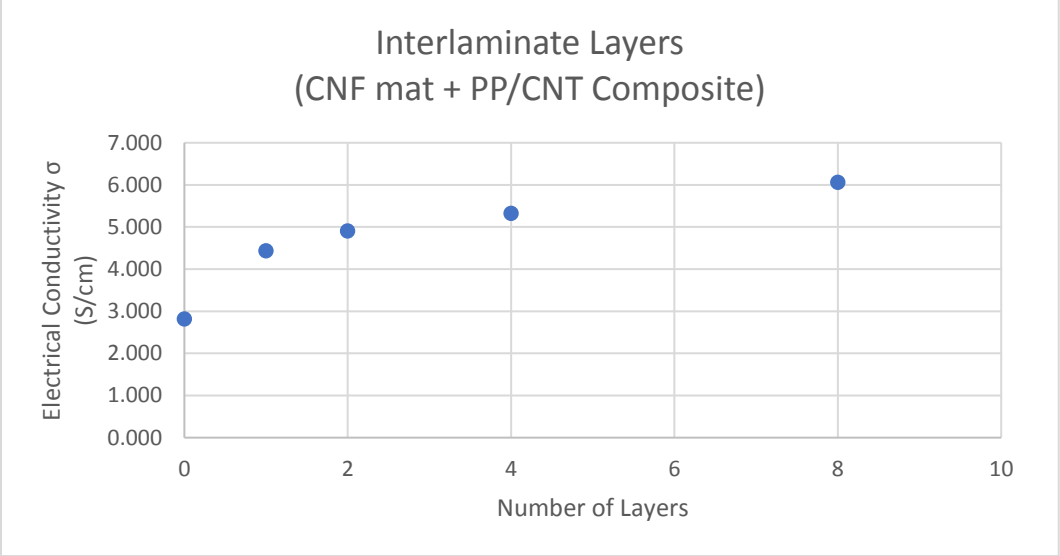

Figure 25. Interlaminate number of Layers vs. Electrical Conductivity. All samples prepared at 1000° C.

5.3 Electromagnetic Interference Shielding Effectiveness (EMI SE)

EMI SE is the capacity of one object to block electromagnetic waves both from natural and manmade sources. The EMI SE values of the materials were obtained using the Hewlett

Packard RF Network Analyzer, which has a frequency test range from .03 MHz to 1.3 GHz. Each sample was held between the two aligned fixtures to be recorded, and the values obtained from the analyzer were given in decibels (dB). The SE was obtained by:

$$SE = 10 \log\left(\frac{P_{load}}{P_{trans}}\right) \quad 4$$

where the SE is the ratio of the power received with the sample load, and the power transmitted without it.

To correctly compare the samples against each other, they were kept at a specific thickness to merely rely on the rest of the variants, except for the interlaminated samples, where the materials were held as the constants, varying the layers and therefore the total thickness of the material. Figure 26 portrays and compares the difference in shielding effectiveness between a single CNF mat and an 8-layered CNF mat, containing .1 weight percent CNT, and PP/15% CNT composite. The 8-layered interlaminated sample was .6 mm in thickness, and it was the most efficient sample obtained regarding EMI SE, being able to shield about 50 dB along the 1300 MHz range.

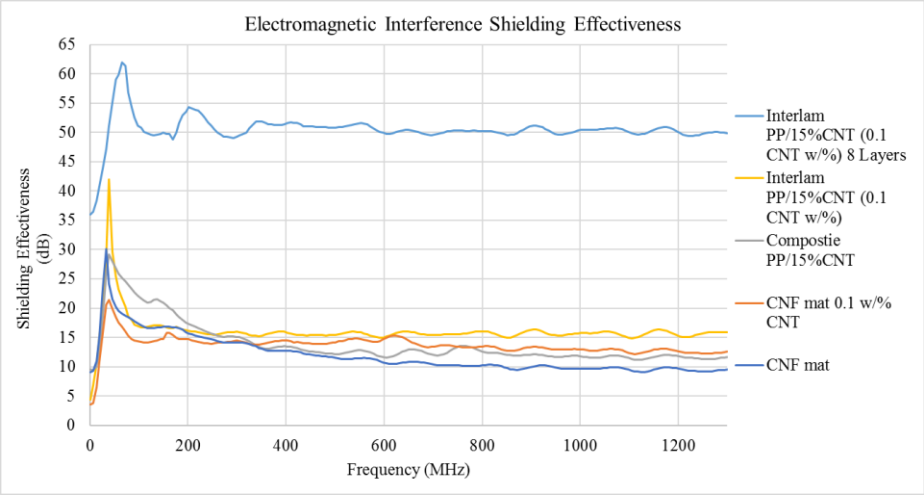

Figure 26. EMI SE of CNF mat and interlaminated carbon systems heat-treated at 1000° C

5.3.1 CNF mats

The EMI SE difference between the CNF mats was not significant, given that they all ranged between 8 and 13 decibels as it can be seen in Figure 27. Figure 27 (b) shows a more focused image of the SE results emphasizing on the frequency range from 800 to 1300 MHz, and it can be observed that there is still a trend followed comparing the SE with the electrical conductivity results.

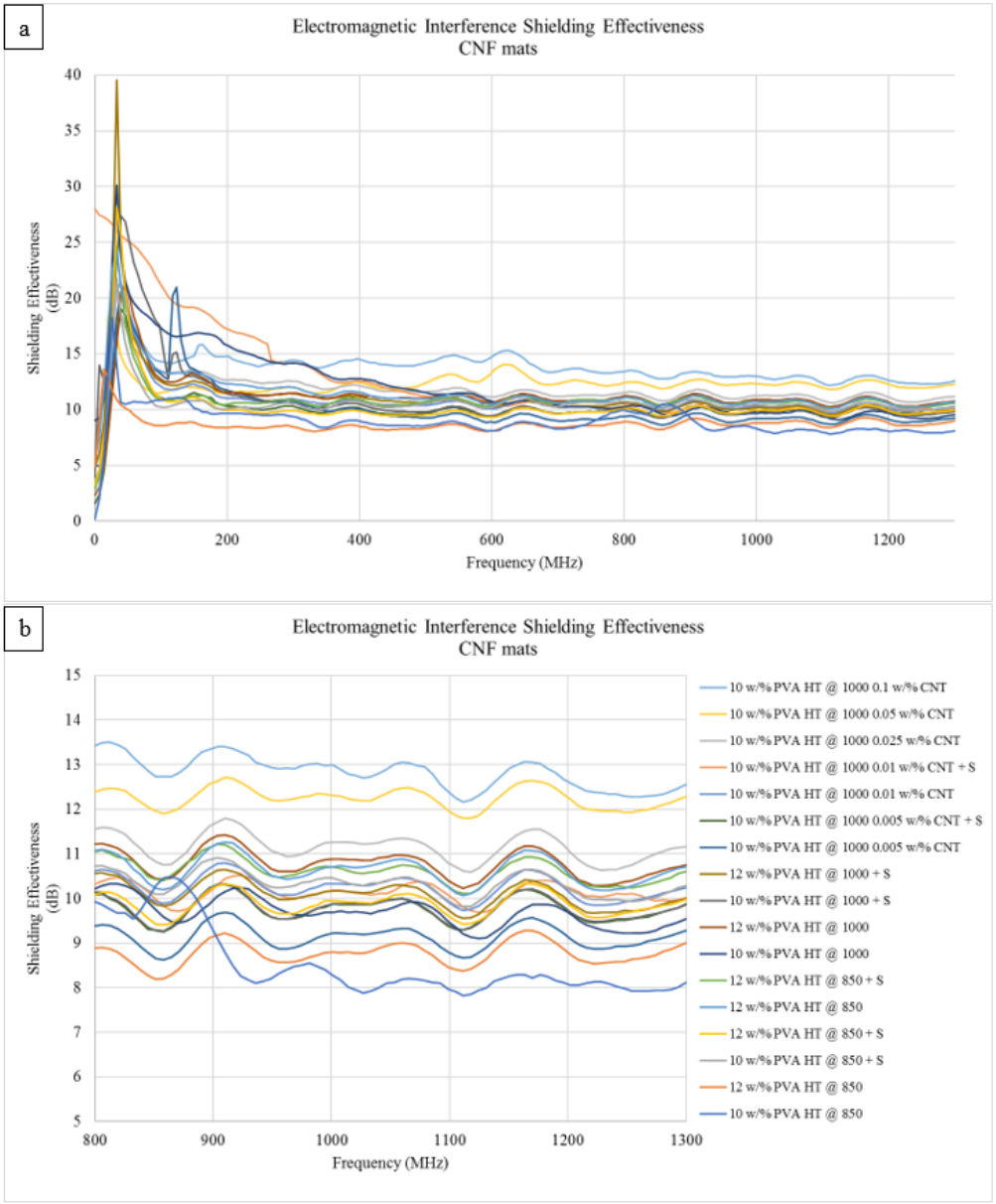

Figure 27. (a) EMI SE for CNF mats; (b) zoomed in portion to frequency 800-1300 MHz

5.3.2 PP/CNT Composite

The PP/CNT composite was created using two different weight ratios of CNT to PP, 12 weight percent, and 15 weight percent. The results for their EMI SE can be observed in Table , and when compared with one another it is established that the difference in ratios is not broad, taking in consideration that conductivity of the material did double from .7 S/cm to 1.49 S/cm.

Table 5. PP/CNT composite EMI SE

	Composite PP/12% CNT	Compostie PP/15% CNT
Freq(MHz)	SE (dB)	SE (dB)
0.3	3.407	9.534
20	12.01	12.366
500	11.305	12.15
1000	11.109	11.778
1300	11.031	11.686

The thickness of the samples used when testing for the SE in Table 5 were about .09 mm. This thickness was used because that is the thickness of the CNF mats and a similar comparison wanted to be achieved.

5.3.3 Interlaminate Carbon Systems

The interlaminated systems proved to be the most effective method to improve the SE. Figure 28 displays how the introduction of laminates impacted the SE at 1300 MHz, with one lamination, the samples endured around 15 dB, and when the laminations were doubled to 2, they could take almost two times as much dB, reaching 30. This might be caused because, at one lamination, the sample's thickness is about .09 mm, and that may mean that the thickness of the sample is much smaller than its skin depth. When this happens, the multiple reflection sides of the SE harms it instead of contributing to withstand more [30]. After the second lamination, the thickness provided for the multiple reflections and absorption mechanisms to improve, while the

reflection mechanisms enhanced because the resistivity of the material decreased impactfully as it was shown in Table 4.

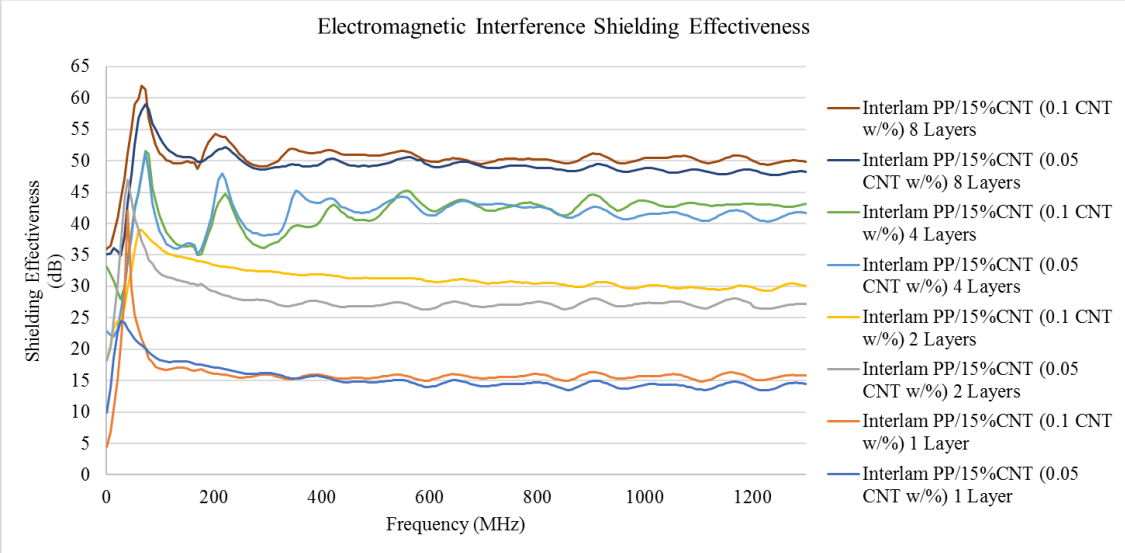

Figure 28. EMI SE of interlaminated carbon systems carbonized at 1000° C

CHAPTER VI

CONCLUSION

CNF mats were created successfully using PVA as a precursor. An optimization method was achieved at ranges of 6000 to 10,000 RPM with collectors at 27cm away from the center of Cyclone Force Spinning Machine. PP/CNT composite samples created in the HAAKE mixer were efficiently impregnated in CNF mats and furthermore combined into interlaminated samples with a thickness of .1mm. The interlaminated carbon systems varied in PVA weight percentage, CNT weight percentage, heat treatment temperature, the addition of sodium chloride for graphitization and more impactfully, the number of layers of interlamination. The different samples were characterized and studied on their electric and electromagnetic properties.

The study successfully established the impact that is applied to the electric conductivity and the EMI SE when a higher speed is utilized when creating fibers, the utilization of salt and MWCNTs in the precursor, different carbonization temperatures are used and when interlamination process is applied. The most efficient interlaminated carbon system was able to display an SE of 50 dB and an electric conductivity of 6 S/cm, improving it over one order of magnitude from that of a single CNF mat.

CHAPTER VII

FUTURE WORK

The recommendations offered for any plans for improving the results obtained in this study would be to find the correct method to incorporate the things that worked together. For example, it was observed that every technique helped to improve the electrical properties and SE of the CNF mats, but they were not capable of working together given that the formation of fibers wouldn't be possible. If the method of adding MWCNTs to the precursor could be applied along with higher PVA weight percentage for the fibers to be able to derive from a higher velocity process, that could potentially improve the properties.

REFERENCES

[1] N. B. Janda, "Development of a Predictive Shielding Effectiveness Model for Carbon Fiber / Nylon Based Composites," no. August, 2004.

[2] L. L. Wang, B. K. Tay, K. Y. See, Z. Sun, L. K. Tan, and D. Lua, "Electromagnetic interference shielding effectiveness of carbon-based materials prepared by screen printing," *Carbon N. Y.*, vol. 47, no. 8, pp. 1905–1910, 2009.

[3] H. Vasquez, L. Espinoza, and K. Lozano, "Simple Device for Electromagnetic Interference Shielding Effectiveness Measurement," *Ieee*, pp. 62–68, 2009.

[4] Y. J. Yang, S. M; Chang, Y. Y; Hsieh, Y. C; Lee, "Electromagnetic shielding effectiveness of multilayer metallic thin film on plastic substrates," *J. Appl. Polym. Sci.*, vol. 110, no. 3, 2008.

[5] S. Yang, K. Lozano, A. Lomeli, H. D. Foltz, and R. Jones, "Electromagnetic interference shielding effectiveness of carbon nanofiber/LCP composites," *Compos. Part A Appl. Sci. Manuf.*, vol. 36, no. 5, pp. 691–697, 2005.

[6] L. D. Cremar, J. Acosta-Martinez, A. Villarreal, A. Salinas, and K. Lozano, "Mechanical and electrical characterization of carbon nanofibers produced from water soluble precursors," *Mater. Today Commun.*, vol. 7, pp. 134–139, 2016.

[7] K. Lozano, "Vapor-grown carbon-fiber composites: Processing and electrostatic dissipative applications," *Jom*, vol. 52, no. 11, pp. 34–36, 2000.

[8] D. D. . Chung, "Electromagnetic interference shielding effectiveness of carbon materials," *Carbon N. Y.*, vol. 39, no. 2, pp. 279–285, 2001.

[9] W. S. Jou, H. Z. Cheng, and C. F. Hsu, "The electromagnetic shielding effectiveness of carbon nanotubes polymer composites," *J. Alloys Compd.*, vol. 434–435, no. SPEC. ISS., pp. 641–645, 2007.

[10] D. Markham, "Shielding: quantifying the shielding requirements for portable electronic design and providing new solutions by using a combination of materials and design," *Mater. Des.*, vol. 21, no. 1, pp. 45–50, 1999.

[11] M. H. Al-Saleh and U. Sundararaj, "Electromagnetic interference shielding mechanisms of CNT/polymer composites," *Carbon N. Y.*, vol. 47, no. 7, pp. 1738–1746, 2009.

[12] J. Wu and D. D. L. Chung, "Improving colloidal graphite for electromagnetic interference shielding using 0.1 μm diameter carbon filaments [2]," *Carbon N. Y.*, vol. 41, no. 6, pp. 1313–1315, 2003.

[13] N. Li *et al.*, "Electromagnetic Interference (EMI) shielding of single-walled carbon nanotube epoxy composites," *Nano Lett.*, vol. 6, no. 6, pp. 1141–1145, 2006.

[14] V. Eswaraiah, V. Sankaranarayanan, and S. Ramaprabhu, "Functionalized graphene-PVDF foam composites for EMI shielding," *Macromol. Mater. Eng.*, vol. 296, no. 10, pp. 894–898, 2011.

[15] M. H. Al-Saleh, W. H. Saadeh, and U. Sundararaj, "EMI shielding effectiveness of carbon based nanostructured polymeric materials: A comparative study," *Carbon N. Y.*, vol. 60, no. 2, pp. 146–156, 2013.

[16] H. Estrada, J. Trovillion, L. S. Lee, M. Tusz, A. Kumar, and L. D. Stephenson, "Electrical properties of fiber and carbon nanotube reinforced polymer composites," *WIT Trans. Eng. Sci.*, vol. 77, pp. 309–320, 2013.

[17] B. Shen, W. Zhai, and W. Zheng, "Ultrathin flexible graphene film: An excellent thermal conducting material with efficient EMI shielding," *Adv. Funct. Mater.*, vol. 24, no. 28, pp. 4542–4548, 2014.

[18] X. Hong and D. D. L. Chung, "Carbon nanofiber mats for electromagnetic interference shielding," *Carbon N. Y.*, vol. 111, pp. 529–537, 2017.

[19] SASOL, "Hydraulic machines." [Online]. Available: http://www.mstworkbooks.co.za/technology/gr9/gr9-technology-06.html.

[20] S. Swapp, "Scanning Electron Microscopy (SEM)." [Online]. Available: https://serc.carleton.edu/research_education/geochemsheets/techniques/SEM.html.

[21] A. Bogner, P. H. Jouneau, G. Thollet, D. Basset, and C. Gauthier, "A history of scanning electron microscopy developments: Towards 'wet-STEM' imaging," *Micron*, vol. 38, no. 4, pp. 390–401, 2007.

[22] E. Allen and L. Rathbun, "Seeing Nanostructures." [Online]. Available: http://www.nnin.org/news-events/spotlights/seeing-nanostructures.

[23] B. Hafner, "Scanning Electron Microscopy Primer," 2007. [Online]. Available: http://www.charfac.umn.edu/.

[24] "How the SEM Works." [Online]. Available: http://antoine.frostburg.edu/engin/sem/workings.html.

[25] "Electron-matter interactions," 2014. [Online]. Available: http://www.ammrf.org.au/myscope/sem/background/concepts/interactions.php.

[26] Hewlett-Packard, “HP 871X and HP 8714C RF Network Analyzers.” .

[27] Hewlett-Packard, “RF Economy Network Analyzers,” 1996. [Online]. Available: https://www.equipland.com/objects/catalog/product/extras/10185_8711C.pdf.

[28] F. M. Smits, “Measurement of Sheet Resistivities with the Four- Point Probe,” *Bell Syst. Tech. J.*, vol. 37, no. 3, pp. 711–718, 1958.

[29] A. Mandana *et al.*, “In Situ Production of Graphene–Fiber Hybrid Structures,” *ACS Appl. Mater. Interfaces*, vol. 9, no. 30, 2017.

[30] H. Garcia, “ELECTROMAGNETIC INTERFERENCE SHIELDING EFFECTIVENESS OF METALLIC THIN FILMS DEPOSITED ON HIGH DENSITY POLYETHYLENE AND STYRENE BUTADIENE COPOLYMER REINFORCED WITH CARBON NANOFIBERS A Thesis HORUS GARCIA Submitted to the Graduate School of the University o,” no. August, 2012.

BIOGRAPHICAL SKETCH

Homero Gonzalez Guardiola, homero.gonzalez89@gamil.com, is originally from Monterrey, Nuevo Leon, Mexico, where he grew up knowing he wanted to be an engineer. In 2005, he moved to McAllen, Texas to improve his English skills. The same year he started working in an amusement park where he rose to become a manager and lead for eight years. In 2008, he enrolled to the University of Texas-Pan American where he would follow his dream and graduate with a Bachelor of Science in Mechanical Engineering. In the summer of 2012, he worked as an engineering intern for GE, but it wasn't until 2013 where he would obtain his first actual engineering position working for John Deere after graduation. In 2015, Homero decided to continue his education and enrolled in The University of Texas Rio Grande Valley. During his time there, he worked as a teacher assistant in various engineering courses, and as a research assistant in the university's polymer/nanotechnology lab. He graduated with a Master's of Science in Mechanical Engineering May 2018.